

Fast determination of saturation intensity and maximum emission rate by single-emitter imaging

J. Y. P. Butter and B. Hecht

Nano-Optics group, National Center of Competence for Research in Nanoscale Science, Institute of Physics, University of Basel, Klingelbergstr. 82, CH-4056 Basel, Switzerland

bert.hecht@nano-optics.ch

Abstract: We investigate the dependence of the spot size in single-emitter confocal imaging on the degree of saturation. We show that single-emitter spots are broadened and flattened significantly already at excitation intensities well below saturation. The resulting single-emitter spot shapes thus deviate significantly from the excitation point spread function. We show and support by Monte Carlo simulations that fitting of a single spot is sufficient to extract the saturation intensity and the maximum emission rate of a single emitter with high accuracy. Our results will be of interest in all areas of single-emitter studies.

© 2006 Optical Society of America

OCIS codes: (180.1790) Confocal microscopy, (300.6280) Spectroscopy, fluorescence and luminescence, (260.2510) Fluorescence, (270.0270) Quantum optics

References and links

1. T. Basché, W. E. Moerner, M. Orrit, and U. P. Wild, eds., *Single-Molecule Optical Detection, Imaging and Spectroscopy* (VCH Verlagsgesellschaft, Weinheim, 1997).
2. W. P. Ambrose, T. Basché, and W. E. Moerner, "Detection and spectroscopy of single pentacene molecules in a *p*-terphenyl crystal by means of fluorescence excitation," *J. Chem. Phys.* **95**, 7150–7163 (1991).
3. L. Novotny and B. Hecht, *Principles of Nano-Optics* (Cambridge University Press, 2006).
4. N. Bobroff, "Position Measurement with a Resolution and Noise-Limited Instrument," *Rev. Sci. Instrum.* **57**, 1152–1157 (1986).
5. T. Schmidt, G. J. Schütz, W. Baumgartner, H. J. Gruber, and H. Schindler, "Imaging of single molecule diffusion," *Proc. Natl. Acad. Sci. USA* **93**, 2926–2929 (1996).
6. A. Bloeiß, Y. Durand, M. Matsushita, H. van der Meer, G. J. Brakenhoff, and J. Schmidt, "Optical far-field microscopy of single molecules with 3.4 nm lateral resolution," *J. Microsc.* **205**, 76–85 (2002).
7. A. M. van Oijen, J. Köhler, J. Schmidt, M. Müller, and G. J. Brakenhoff, "3-Dimensional super-resolution by spectrally selective imaging," *Chem. Phys. Lett.* **292**, 183–187 (1998).
8. A. Yildiz, J. N. Forkey, S. A. McKinney, T. Ha, Y. E. Goldman, and P. R. Selvin, "Myosin V Walks Hand-Over-Hand: Single Fluorophore Imaging with 1.5-nm Localization," *Science* **300**, 2061–2065 (2003).
9. J.-M. Segura, A. Renn, and B. Hecht, "A sample-scanning confocal optical microscope for cryogenic operation," *Rev. Sci. Instrum.* **71**, 1706–1711 (2000).
10. S. Kummer, F. Kulzer, R. Kettner, T. Basché, C. Tietz, C. Glowatz, and C. Kryschi, "Absorption, excitation and emission spectroscopy of terrylene in *p*-terphenyl: Bulk measurements and single molecule studies," *J. Chem. Phys.* **107**, 7673–7684 (1997).
11. S. Kummer, T. Basché, and C. Bräuchle, "Terrylene in *p*-terphenyl: a novel single crystalline system for single molecule spectroscopy at low temperatures," *Chem. Phys. Lett.* **229**, 309–316 (1994).
12. P. Bordat and R. Brown, "Molecular mechanisms of photo-induced spectral diffusion of single terrylene molecules in *p*-terphenyl," *J. Chem. Phys.* **116**, 229–236 (2002).
13. J. Y. P. Butter and B. Hecht, "Aperture scanning near-field optical microscopy and spectroscopy of single terrylene molecules at 1.8 K," *Nanotechnology* **17**, 1547–1550 (2006).

14. T. Plakhotnik, W. E. Moerner, V. Palm, and U. P. Wild, "Single molecule spectroscopy: maximum emission rate and saturation intensity," *Opt. Commun.* **114**, 83–88 (1995).
 15. J. Bernard, L. Fleury, H. Talon, and M. Orrit, "Photon bunching in the fluorescence from single molecules: A probe for intersystem crossing," *J. Chem. Phys.* **98**, 850–859 (1993).
 16. H. de Vries and D. A. Wiersma, "Photophysical and photochemical molecular hole burning theory," *J. Chem. Phys.* **72**, 1851–1863 (1980).
 17. P. Brémaud, *An introduction to probabilistic modeling* (Springer-Verlag, 1994).
 18. P. R. Bevington and D. K. Robinson, *Data reduction and error analysis for the physical sciences*, 2nd ed. (WCB/McGraw-Hill, 1992).
-

1. Introduction

The determination of the saturation parameters is vital in single-emitter studies to establish well-defined experimental conditions [1]. Under saturation the background count rate usually increases faster than the emission rate of the single emitter eventually degrading the signal-to-noise ratio. Furthermore, under saturation the maximal cycling rate between the emitter's excited and ground states leads to strong thermal energy dissipation as well as to a maximal probability for photo-chemical processes leading to irreversible bleaching to occur. For emitters with narrow absorption lines excited by narrow-band lasers, as is typical for single molecules at low temperature, saturation effects are of particular importance since saturation intensities under such circumstances are extremely low. We consider such a case in the following. However, our results are applicable to any single-emitter system.

In a traditional saturation experiment using a single emitter with a narrow absorption line, excitation spectra are recorded at different excitation intensities including intensities presumably well above saturation. To determine the saturation parameters from such data, the obtained resonance curves are fitted with Lorentzians, with line-width and amplitude as main fitting parameters. Plotting line width and amplitude vs. the excitation intensity allows us to extract the homogeneous line width, the saturation intensity and the maximum emission rate by fitting the equations for saturation of the corresponding three-level system [2]. Disadvantages of this method are (i) the long measurement time per saturation curve and (ii) the high intensities the emitter is subjected to, which often leads to irreversible spectral changes and/or photobleaching. As a consequence, the particular emitters that had been used to determine saturation parameters are usually lost for further experiments. Furthermore, saturation parameters are often subject to large errors and results are dominated by particularly photostable molecules that survive the saturation experiment but do *not* represent the "typical" emitter in the sample.

In this letter we introduce a simple and fast method to determine the saturation parameters of individual emitters. The method does not require strong excitation of the emitter far above the saturation intensity. It relies on nonlinear fitting of the single emitter's image spot typically yielding its amplitude, position, and width. Because of the image spot's bell-shaped intensity distribution, position and width can be determined with extraordinary precision down to a few nanometers [3]. While the *position sensitivity* provided by such a fitting procedure has been pointed out earlier [4] and was exploited in various experiments [5, 6, 7, 8] the accuracy in determining the width of a spot has not been addressed. We experimentally show that the saturation parameters of a single emitter can be extracted from the increased width of a single image spot recorded at a fixed excitation intensity well below the saturation intensity.

To this end microscopy images of single terrylene molecules at different excitation frequencies covering the spectral line of a molecule at several different excitation intensities were recorded. All spots are fitted with two-dimensional Gaussians providing the amplitude, the half width at half maximum (HWHM), the position, and the background-level of each spot. Based on such a set of data our new method is compared to the traditional saturation experiment. Realistic Monte Carlo simulations are performed to check that the observed effects are not caused

by fitting artifacts.

2. Experimental

The experiments are performed on a home-built scanning confocal optical microscope operating at 1.8 K in a He-bath cryostat. Details are described elsewhere [9]. In brief, excitation light is provided by a single-mode ring dye-laser (Coherent 699-21, Rhodamine 6G) pumped by an argon-ion laser. After power-stabilization a small fraction of the circularly polarized light ($\sim 4\%$) is reflected by a glass wedge mounted at a shallow angle and enters the cryostat via a window at the bottom. The excitation light is focused onto the sample by a microscope objective (Microthek, 0.85 NA, $60\times$) which resides in the superfluid helium.

The fluorescence and backscattered light are collected by the same objective and transmitted by the glass wedge (96% transmission). The light is filtered spectrally by a holographic Notch filter and the Stokes-shifted fluorescence is focused onto an avalanche photodiode (SPCM-AQR13). At cryogenic temperature, the sample can be scanned over ranges of up to $34 \times 34 \mu\text{m}^2$ using a bimorph scanner located in the superfluid helium. The laser frequency can be scanned continuously or in steps of 10 MHz over ranges of up to 25 GHz.

The measurements were performed on single molecules of terrylene in *p*-terphenyl. Crystalline samples of *p*-terphenyl doped with a small amount of terrylene were grown in a co-sublimation process [10]. Crystal flakes with lateral sizes of up to several millimeters and of about $10 \mu\text{m}$ in thickness were used that adhered to clean glass cover-slips by Van der Waals forces.

All measurements were performed on the zero-phonon line of the lowest singlet-singlet transition of terrylene in *p*-terphenyl in the O_2 site at about 578.5 nm. Molecules in this site are spectrally stable and well suited for single molecule spectroscopy at cryogenic temperature. They have an orientation that is almost perpendicular to the crystal surface [11, 10, 12]. However, from aperture scanning near-field optical microscopy studies on these crystals [13], we know that there exist molecules sitting at defect sites having differing orientations. Molecules with a transition dipole moment with a smaller angle to the sample surface appear brighter in images, as the different orientation of their transition dipole moments leads to a lower saturation intensity and an improved collection efficiency of the fluorescence [14]. Therefore, an experimental bias exists towards the observation of molecules sitting at defects.

3. Theory

Single molecules may be considered point sources. The image of a single molecule in a scanning confocal optical microscope at intensities far below saturation therefore reflects the shape of the excitation point spread function [3]. Thus for excitation with a Gaussian beam, the shape of the molecule's image spot is expected to be a Gaussian as well.

Analysis of saturation measurements from spectral data is usually based on a theoretical description of the saturation of single molecules [15] which follows the work by De Vries and Wiersma [16] for a three level system in which the corresponding optical Bloch equations are solved. From the steady-state solution, a relation between the fluorescence emission rate R of a single absorber and the excitation intensity is derived [2]:

$$R(I) = R_{\infty} \cdot \frac{I/I_S}{1 + I/I_S} \quad (1)$$

where R_{∞} denotes the maximum emission rate, I the excitation intensity and I_S the saturation intensity.

Equation (1) can be used to include the effect of saturation in the description of a single-molecule image spot obtained e.g. by a confocal microscope. For a Gaussian excitation point

spread function, Eq. (1) can be rewritten as:

$$R'(x, y, A) = R_{\infty} \cdot \frac{A \cdot e^{-\frac{(x-x_0)^2 + (y-y_0)^2}{2\xi^2}}}{1 + A \cdot e^{-\frac{(x-x_0)^2 + (y-y_0)^2}{2\xi^2}}} \quad (2)$$

where R' denotes the emission rate as a function of position and relative intensity, R_{∞} the maximum emission rate, $A = I/I_S$ the relative intensity as a function of the saturation intensity, x and y the positions with respect to the molecule's position (x_0, y_0) , and ξ the width of 1 standard-deviation of the Gaussian excitation spot (a constant). Even at intensities close to but still below the saturation intensity of the molecule, the image spot as defined by Eq. (2) deviates slightly but measurably from the ideal Gaussian shape showing a “flattening” and broadening. For excitation intensities above the saturation intensity, these effects become very pronounced.

We conclude that in case the true point-spread function of the microscope, i.e. ξ , is sufficiently well characterized, e.g. by imaging a molecule far below saturation or far out of resonance, fitting of Eq. (2) to a *single* spot can be used to determine the maximum emission rate R_{∞} and the saturation intensity via the parameter A .

4. Results and discussion

To obtain both classical saturation data and saturation data based on the proposed “spot size method” we recorded a matrix of single-molecule images as a function of both excitation frequency and intensity. Frequency-dependent images were recorded at five different intensities. Fig. 1 summarizes the results of the classical data evaluation. Fig. 1(A) shows the spectral line of the molecule at two different excitation intensities, below (6.8 W/cm^2) and above saturation (67.6 W/cm^2). The lines were constructed from the amplitudes of two-dimensional Gaussians that were fitted to the measured single-molecule image spots. Gaussian curve fitting was used to quantify the observed effects. The width of 1 standard-deviation of the Gaussian was taken as the HWHM throughout the experiment. The error bars represent the uncertainties obtained from the Gaussian fit. The uncertainties are largest close to the resonance of the line recorded at the higher intensity. This effect is due to the increased occurrence of blinking close to the resonance. The spectral lines are identical to the ones that would have been observed by scanning the laser frequency over the resonance of the molecule residing in the confocal volume. From all such spectral lines, a saturation curve of emission rate vs excitation intensity was constructed, as is shown in Fig. 1(B). The saturation intensity as determined by fitting to Eq. (1) was $I_S = 9.8 \pm 0.8 \text{ W/cm}^2$. This intensity is clearly lower than the expected saturation intensity, 22.7 W/cm^2 , for a single terrylene molecule in a *p*-terphenyl crystal [11]. We ascribe the discrepancy to the presence of defects in the crystals, which leads to molecules having aberrant orientations [14]. In our samples such molecules were observed rather frequently. Once the saturation intensity is known, relative intensities may be used as indicated on the upper horizontal axis of Fig. 1(B).

The HWHM of the spots as a function of detuning is shown at two intensities in Fig. 1(C). Remarkably, a significant increase of spot-size around the resonance is observed even at the lowest intensity which is only on the onset of saturation ($I = 0.7 \cdot I_S$). As mentioned before the effect of blinking causes an increase in the uncertainties of the measured spot-sizes at higher intensity close to resonance. The increase in spot-size at large negative detuning for $I = 6.9 \cdot I_S$ is explained by the decreasing signal-to-background ratio. The low intensity data demonstrate that the effect of saturation on the measured spot size is already present and significant at comparably low intensities.

Finally, the measured spot-size in resonance is plotted as a function of relative intensity in Fig. 1(D). A clear increase in spot-size is observed. The uncertainty on the HWHM increases

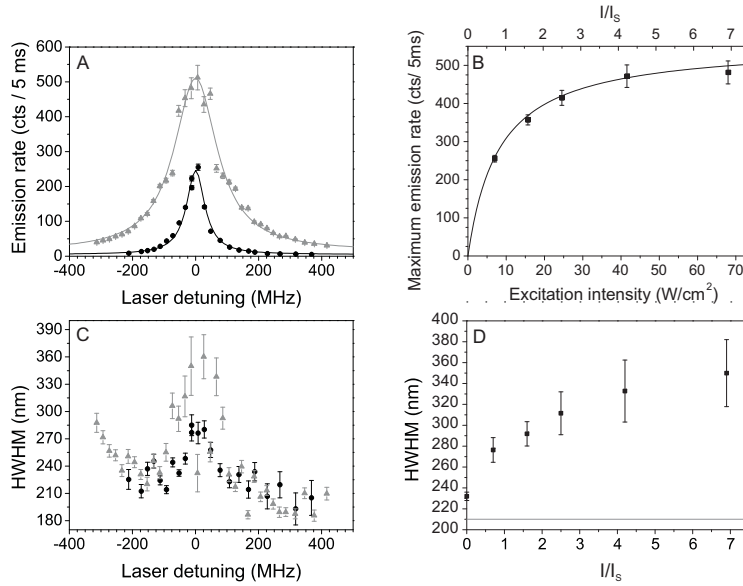


Fig. 1. Classical saturation obtained from a frequency and intensity dependent single-molecule images. (A) Spectral lines of a single molecule at two different intensities. (B) Saturation curve of the same molecule. The lower horizontal axis shows the excitation intensity whereas the upper horizontal axis shows the relative intensities as a function of saturation intensity. (C) Change in the observed HWHM of the imaged spot of the molecule as a function of detuning. The black circles denote the values for $I = 0.7 \cdot I_S$ and the grey triangles for $I = 6.9 \cdot I_S$. (D) HWHM of the spot in resonance as a function of relative intensity. The spot-size at zero intensity is the measured spot size far out of resonance. The solid grey line denotes the calculated point spread function, which doesn't take into account any effect due to the presence of superfluid helium. The integration time was 5 ms per pixel.

with intensity and is caused by the increased amount of blinking in the spots at higher intensities.

To gain insight in the accuracy of the determination of spot sizes of single molecules and to estimate the influence of saturation on the observed spot sizes, a Monte Carlo simulation was performed. Pseudo-random numbers with a Poisson distribution are used to simulate measurement noise. The simulation addresses the question whether the given spot size of such a noisy spot below saturation is recovered by fitting with a Gaussian, even when the detuning increases and thus the signal-to-background ratio decreases. The simulation was run in Mathematica (Wolfram research). The simulation addresses the question in a negative testing scheme, i.e. a constant spot size is used as input. Detuning from resonance results in a decreased signal-to-background level. Spectrally, a single molecule is characterized by a homogeneous line with a Lorentzian shape. The detected emission rate per integration time, R_1 , as a function of detuning, f , is described by:

$$R_1(f) = R_0 + \frac{H}{4 \cdot \frac{(f-f_0)^2}{W^2} + 1} \quad (3)$$

where R_0 is the off-set of the background level from 0, H the amplitude, f_0 the resonance frequency and W the Full Width at Half Maximum (FWHM). As input values, $R_0 = 0$ counts per integration time, $H = 200$ counts per integration time, and $W = 60$ MHz were chosen, which

represent realistic values typically found in the experiment.

In microscopy images, the molecule is seen as a Gaussian spot, reflecting the shape of the excitation point spread function. Assuming this spot to be located at (0,0), it is described as a function of position, detuning and size:

$$\text{spot}(x,y,f,\xi) = R_1(f) \cdot e^{-\frac{x^2+y^2}{2\xi^2}} \quad (4)$$

where x and y denote the x - and y -coordinates, respectively, and ξ is a measure for the HWHM of the spot, corresponding to the width of 1 standard-deviation of a Gaussian. ξ was set to 4.16 pixels in all simulations. $R_1(f)$ was defined in Eq. (3) and takes into account the spectral dependence of the amplitude of the spot. The function $\text{spot}(x,y,f,\xi)$ defines an ideal spot below saturation without noise on zero background. The signal noise is described by a Poisson distribution, which has as mean (μ) corresponding to the signal amplitude and the variance (σ^2) [17, 18]. The background is defined as a Poisson distribution with mean 8.

Exploiting the symmetry of the problem only positive values of the detuning were used in the simulation. For each of 8 different spectral positions studied, 1000 spots were generated. Each spot was fitted with the following Gaussian function:

$$\text{fit}(x,y) = a + b \cdot e^{-\frac{x^2+y^2}{2c^2}} \quad (5)$$

where the parameter a represents the background level, b the amplitude of the spot and c the HWHM of the spot in exactly the same way as ξ . From Eq. (5) it is obvious that center positions of the spot that are different from the origin are not considered. Initially this was taken into account by two additional parameters, however, due to the extremely small values (on the order of 10^{-3} to 10^{-4}) that resulted from a first run of the simulation and the huge increase of calculation time, this was omitted in further runs of the simulation.

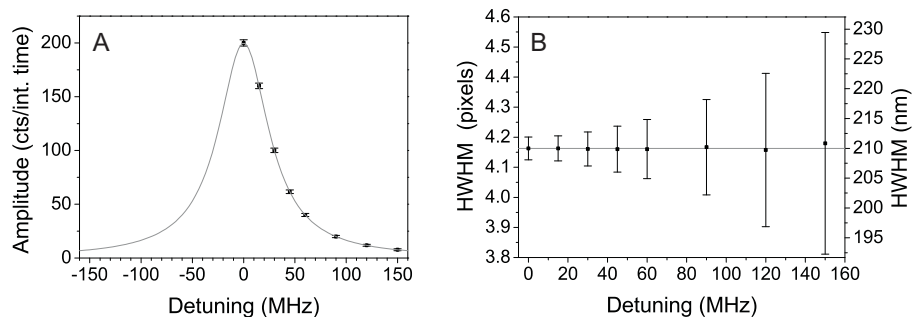


Fig. 2. Results of the Monte Carlo simulation on the spot-size as a function of detuning below saturation. (A) The average amplitudes with corresponding uncertainties as a function of detuning (squares) and the input values (grey line). (B) The influence of detuning on the HWHM, both absolute in pixels (left axis), with the corresponding input value as a grey line, and in nm assuming a diffraction limited spot size.

The thus generated fitting results of 1000 spots per detuning were used to generate distributions of the amplitude, b , and the HWHM, c , as a function of detuning. The distributions of the amplitudes with corresponding uncertainties were used to check whether the input was reproduced, as is shown in Fig. 2(A). The solid grey line represents the input as defined by Eq. (3), whereas the dots with error bars show the average amplitudes with corresponding standard deviations that came out of the simulation. A good agreement is found.

The distributions of the widths and corresponding uncertainties constitute the main result of the simulation and answer the question whether an observed change in spot size is an artefact from the fitting procedure or not. The distributions of widths at each detuning are shown in Fig. 2(B). It shows the HWHM as a function of detuning as square dots with corresponding error bars and the input value, $\xi = 4.16$ pixels as a solid grey line. The result demonstrates that at larger detuning, i.e., lower signal-to-background ratio, the uncertainties on the HWHM increase strongly, while the mean value remains extremely close to the input value. The influence of any systematic fitting artefact can be excluded due to the fact that the points are uniformly distributed around the input value. For comparison, the largest variation from the input value is about 0.02 pixels, which would amount to less than 1 nm for a diffraction limited spot. This means that a constant spot size as input is recovered in the fitting process with high accuracy and that any increase in spot size observed experimentally at resonance is caused by a physical process. The large error bar of ~ 15 nm at a detuning of 150 MHz indicates that for lower signal-to-background ratio, i.e. in the wing of the line, the uncertainty on the obtained values increases.

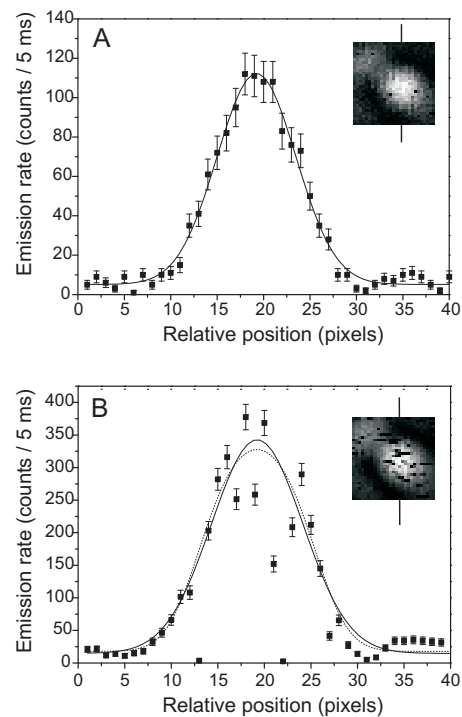


Fig. 3. Illustration of the determination of the saturation intensity and the maximum emission rate from 2 spots of a single molecule at the intensity $I = 0.7 \cdot I_S$. (A) shows the line-profile of the non resonant spot through the center and (B) of the resonant spot. The insets show normalized images, $1.3 \times 1.3 \mu\text{m}$ in size, of the respective spots. The lines indicate where the line-cut was taken. The solid lines represent Gaussian fits to the data, whereas the dotted line is a fit with Eq. (2).

An important consequence of the change in measured spot size, which is shown by the simulation to be no fitting artefact, is illustrated in Fig. 3. It shows the line-cuts and images of a single molecule recorded at the intensity $I = 0.7 \cdot I_S$. The data shown in Fig. 3(A) is recorded

at a detuning of -60 MHz. The data points in the line cut are represented by dots, whereas the error-bars denote the amplitudes of the shot-noise on the data. From Fig. 1(C) it is clear that the spot size at this detuning was typical for the molecule (far) out of resonance, even at high intensities. The spot in this image was fitted with a Gaussian, yielding ξ . Fig. 3(B) shows the data from the same molecule in resonance. The spot was fitted with both a Gaussian curve (solid line) and with Eq. (2) (dotted line). In the latter, ξ was kept fix at the value found from fitting the out-of-resonance image with a Gaussian. The points in which the molecule was blinking (black pixels) were not taken into account during the fitting with both equations. As is seen in Fig. 3(B), significant differences between the fits exist even at an intensity below the saturation intensity. It means that the effects of saturation are already present in the spot. The data is better described by Eq. (2), which has a smaller amplitude and a broader width. This is obvious from the values of χ^2 for the fits, which yield $\chi^2 = 3 \cdot 10^6$ for fitting to Eq. (2) and $\chi^2 = 2 \cdot 10^8$ for fitting to a Gaussian, respectively.

From the fit to Eq. (2) using ξ obtained from Fig. 3(A), the saturation intensity and the maximum emission rate of the molecule were determined, yielding $I_S = 9.1 \pm 2.7$ W/cm² and $R_\infty = 560 \pm 114$ counts/5 ms in perfect agreement with the values obtained from the classical analysis. The accuracy of these values is slightly less than that obtained with the classical method. However, it should be noted that the data were obtained much faster and did not require excitation of the molecule at intensities above saturation.

5. Conclusion

Saturation effects in the images of single molecules are pronounced. Even at intensities that are still below the saturation intensity, the images of a single molecule show a larger spot size than they would show at extremely low intensities or, in the low temperature case, when imaged far out of resonance. This finding is supported by Monte Carlo simulations. The effect is exploited to determine the saturation intensity and maximum emission rate of a single molecule using a single microscopy image only, provided the point-spread function is known. The good agreement of the results with the values obtained from “traditional” spectral saturation analysis demonstrates the power of the method. Our method eliminates the need of recording many spectra of a single molecules, including those at intensities (far) above the saturation intensity. The here proposed method is much faster both in the experiment and in the analysis and is also suited for emitters which don't have narrow absorption lines.

Acknowledgements

The authors are grateful to H.-J. Güntherodt for continuous support. Helpful discussions with S. Karotke, A. Lieb, and D.W. Pohl are acknowledged. Financial support by the Swiss National Science Foundation via a professorship for one of the authors (B.H.) is gratefully acknowledged.